The Astrophysical Journal Letters, 881:L38 (7pp), 2019 August 20 https://doi.org/10.3847/2041-8213/ab3663

Exotic Carbon Chemistry in a Planetary Nebula: The Unusual Case of K4-47

D. R. Schmidt[1,2] and L. M. Ziurys[1,3]
[1] Department of Astronomy and Steward Observatory, University of Arizona, 933 North Cherry Avenue, Tucson, AZ 85721-0065, USA
[2] Department of Physics and Astronomy, Swarthmore College, 500 College Avenue, Swarthmore, PA 19081-1397, USA
[3] Department of Chemistry and Biochemistry, University of Arizona, 933 North Cherry Avenue, Tucson, AZ 85721-0065, USA
Received 2019 May 10; revised 2019 July 26; accepted 2019 July 29; published 2019 August 20

Abstract

Millimeter molecular line observations have been conducted toward the young (∼900 yr) bipolar planetary nebula (PN) K4-47, using the 12 m antenna and the Submillimeter Telescope of the Arizona Radio Observatory, and the Institut de Radioastronomie Millimétrique 30 m Telescope. Measurements at 1, 2, and 3 mm of multiple transitions were carried out to ensure the accuracy of all molecular identifications. K4-47 was found to be unusually chemically rich, containing three complex species, CH_3CN, H_2CNH, and CH_3CCH, which have never before been observed in a planetary nebula. In addition, HC_3N, N_2H^+, H_2CO, c-C_3H_2, and SiO have been identified in this object, as well as a variety of ^{13}C-substituted isotopologues ($H_2{}^{13}CO$, c-$^{13}CCCH_2$, c-$CC^{13}CH_2$, $CH_3{}^{13}CN$, $^{13}CH_3CN$, $CH_3{}^{13}CCH$, and $^{13}CH_3CCH$), including all three doubly^{13}C-substituted varieties of HC_3N—the first known object in which all three species have been detected. After CO and H_2, the most abundant molecules in K4-47 are CCH and CN, which have abundances of $f \sim 8 \times 10^{-7}$, relative to molecular hydrogen. Surprisingly, the next most abundant molecule is CH_3CCH, which has $f \sim 6 \times 10^{-7}$, followed by HCN with an abundance of $\sim 5 \times 10^{-7}$. The results suggest that K4-47 is the most chemically complex planetary nebula currently known. The molecular content of K4-47 closely resembles that of the C-star IRC+10216, but with lower abundances, except for HCO^+, H_2CO, and CH_3CCH. The PN also chemically and morphologically resembles the bipolar protoplanetary nebula CRL 618, with similar enrichments of ^{13}C, ^{15}N, and ^{17}O, suggestive of an explosive process at the end of the asymptotic giant branch.

Key words: astrochemistry – ISM: molecules – nuclear reactions, nucleosynthesis, abundances – planetary nebulae: individual (K4-47) – radio lines: ISM

1. Introduction

The molecular content of planetary nebulae (PNe) has long been thought to be simple and short-lived. Remnant molecules from the asymptotic giant branch (AGB) stage were expected to be photodissociated by the intense ultraviolet (UV) radiation field from the central white dwarf on rapid timescales within several thousand years (Redman et al. 2003). As a result, gas-phase PN ejecta have historically been considered to be atomic in nature, with the cycling of molecular material undergoing a sharp discontinuity.

Recent millimeter observations of PNe, however, have shown the contrary, even into the late stages of nebular evolution. The Helix Nebula, one of the oldest known PNe (age ∼11,000 yr; Meaburn et al. 2008), hosts a surprising variety of molecules with widespread distributions, including HCN, CN, HNC, HCO^+, CCH, c-C_3H_2, and H_2CO (Zack & Ziurys 2013; Schmidt & Ziurys 2017a; Schmidt et al. 2018b). Toward the younger objects NGC 7027 and NGC 6537, species such as SO, H_2CO, CS, N_2H^+, and even HC_3N have been found (Zhang et al. 2008; Edwards & Ziurys 2013). SiO and SO_2 have been detected in the oxygen-rich, middle-aged PN M2-48, as well as CN, HCN, HNC, CS, SO, HCO^+, and N_2H^+(Edwards & Ziurys 2014). More recently, the presence of HCN, HCO^+, HNC, and CCH has been established in 10 other PNe with varied morphologies and spanning a 10,000 yr age range (Schmidt & Ziurys 2016, 2017a, 2017b). In the odd 20 PNe studied at millimeter wavelengths, the most complex species detected thus far contain five atoms: HC_3N and c-C_3H_2. In contrast, C_{60} has been identified in the infrared (IR) in a few PNe (e.g., Cami et al. 2010; García-Hernández et al. 2012), suggesting that molecules with 6–60 atoms may also exist in these objects.

One PN of recent interest is K4-47. This young bipolar nebula (∼400–900 yr post-protoplanetary nebula (PPN) phase) is highly collimated, as indicated in vibrationally excited H_2 (Akras et al. 2017). It has a hot central core traced by highly excited atomic lines such as [O III], with high-velocity lobes at the tips of the outflow, visible in [N II] and [S II] (e.g., Corradi et al. 2000). For many years, the only molecular emission known in this object was from CO and H_2 (Lumsden et al. 2001; Huggins et al. 2005), but newer studies have revealed the presence of CS, HCO^+, HCN, HNC, CCH, and even HC_3N, suggesting a very carbon-rich object (Edwards et al. 2014; Schmidt & Ziurys 2016, 2017a, 2017b; Schmidt et al. 2018a). Perhaps more striking are the anomalous isotope ratios recently found in K4-47, with $^{12}C/^{13}C = 2.2 \pm 0.8$, $^{14}N/^{15}N = 13.6 \pm 6.5$, and $^{16}O/^{17}O = 21.4 \pm 10.3$ (Schmidt et al. 2018a). The apparent C-rich nature of this source, coupled with its low $^{12}C/^{13}C$ ratio, suggests that K4-47 possessed a J-type progenitor star. The excessive enhancement of ^{15}N and ^{17}O and the bipolar geometry also indicates that some explosive process occurred in the object.

To further probe the chemical content of this unusual PN, we have conducted additional molecular observations of K4-47. To our surprise, we have found even more complex species in this source, as well as a significant number of unidentified lines and rare ^{13}C-substituted compounds. In this Letter, we will present these new data and discuss their implications.

2. Observations

Observations were carried out using the 12 m Atacama Large Millimeter/submillimeter Array (ALMA) prototype antenna and Submillimeter Telescope (SMT) of the Arizona Radio Observatory (ARO), as well as the Institut de Radioastronomie Millimétrique (IRAM) 30 m facility. The ARO data reported in this work were obtained between 2013 October and 2018 November. The ARO 12 m measurements utilized a

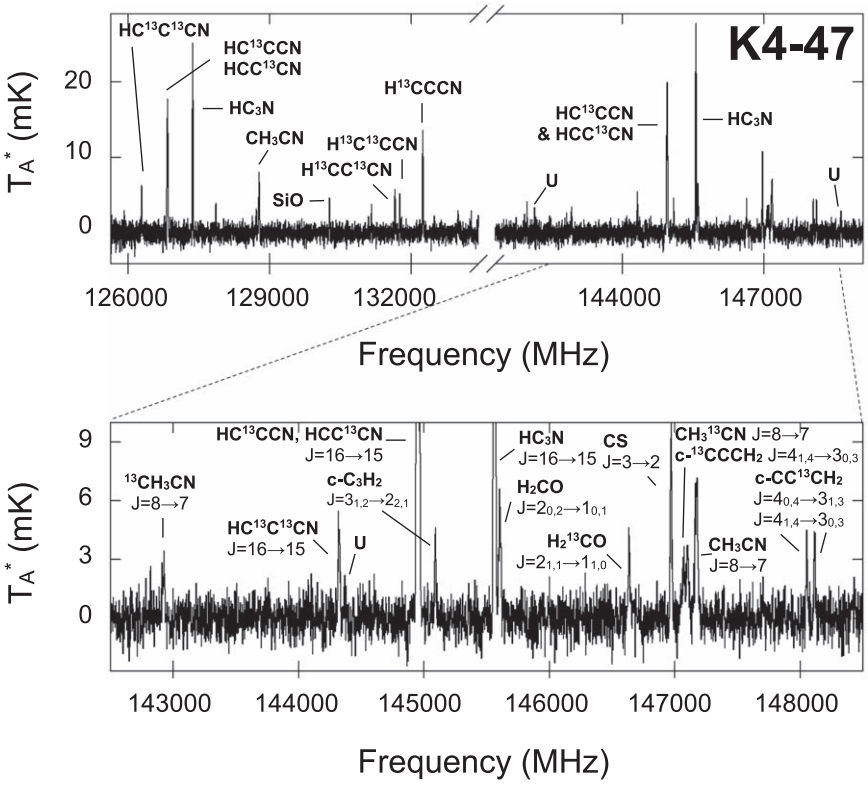

Figure 1. Representative spectra of K4-47, measured with the IRAM 30 m. The top panel displays the full spectrum between ∼125.6 and ∼133.4 GHz (lower sideband) and ∼141.3 and ∼149.1 GHz (upper sideband). Various lines of HC_3N and its ^{13}C-substituted species are apparent in the data as well as some unidentified ("U") lines. The lower panel shows an expanded version of a section of the USB spectrum, identifying features arising from H_2CO, c-C_3H_2, and CH_3CN. All spectra are smoothed to 2 MHz resolution. A V_{LSR} of -27.0 km s^{-1} was assumed. Many of the molecular identifications are new discoveries in PNe, including CH_3CN.

dual-polarization, 3 mm receiver, which employs ALMA Band 3 sideband-separating (SBS) mixers. The image rejection was >16 dB, intrinsic in the mixer architecture, beam sizes covered the range ∼55″–77″, and system temperatures typically varied between T_{sys} ∼ 110–170 K, SSB. A dual-polarization, 1.3 mm receiver was operated at the SMT, consisting of ALMA Band 6 SBS mixers with image rejection >15 dB. Filterbanks with 1 MHz resolution were used as backends at both facilities. Beam sizes were ∼33″–35″, with T_{sys} ∼170–260 K. The IRAM measurements were conducted between 2017 December and 2018 November. All observations were performed using the Eight Mixer Receiver (EMIR) operating in the 2 mm band (∼125–178 GHz) with dual-polarization SBS mixers. The primary backends utilized were the Fourier Transform Spectrometer (FTS) and the wideband autocorrelator WILMA, operated with 200 kHz and 2 MHz resolutions, respectively. Beam sizes for these observations were ∼14″–19″ with T_{sys} ∼80–150 K. The temperature scale for all measurements is T_A^*, determined by the chopper wheel method. The main beam brightness temperature, T_R, is then defined as $T_R = T_A^*/\eta_b$ at ARO, and $T_R = T_A^*\eta_{fss}/\eta_b$ at IRAM, where η_b and η_{fss} are the main beam and forward scattering efficiencies, respectively.

All measurements were taken toward the central position for K4-47 at $\alpha = 04{:}20{:}45.2$; $\delta = 56{:}18{:}12$ (J2000) in beam-switching mode with a subreflector throw of ±2′ at the ARO facilities and ±40″ at the IRAM 30 m. The nominal local standard of rest (LSR) velocity of K4-47 is -27 km s^{-1}. Pointing and focus were determined by observations of planets or quasars such as 0355+508. Typical pointing accuracies for all facilities were ±2″. Local oscillator shifts were performed at all frequencies to eliminate image contamination.

3. Results

In addition to the past observations of various molecules (e.g., Schmidt & Ziurys 2017a, 2017b), a surprising number of new chemical compounds were identified in K4-47 using the Cologne Database for Molecular Spectroscopy (CDMS; Müller et al. 2001, 2005; Endres et al. 2016) and Jet Propulsion Laboratory (JPL; Pickett et al. 1998) databases, as shown in Figures 1 and 2. Among these identifications are SiO, H_2CO, c-C_3H_2, and numerous ^{13}C isotopologues. Three new species, CH_3CN, CH_3CCH, and H_2CNH, had not been detected previously in PNe.

Figure 1 presents sample IRAM spectra in the frequency ranges ∼126–133 GHz and ∼141–149 GHz. The top panel shows all these data, while the lower panel displays an expanded view of the spectrum between 142.5 and 148.5 GHz. Of note in the top spectrum are lines arising from SiO and many ^{13}C singly and doubly substituted isotopologues of HC_3N. Visible in the lower panel are the $J = 8 \rightarrow 7$ transitions of CH_3CN, $CH_3{}^{13}CN$, and $^{13}CH_3CN$, lines of H_2CO, $H_2{}^{13}CO$, c-C_3H_2, c-$^{13}CCCH_2$, and c-$CC^{13}CH_2$, and one unidentified feature labeled "U."

Figure 2 presents individual spectra of the new molecular identifications. Two a-type and one b-type components of the $J = 2 \rightarrow 1$ transition were detected for H_2CNH (also see Table 1); two are shown in Figures 2(c) and (d). For CH_3CCH, the $J = 8 \rightarrow 7$, $9 \rightarrow 8$, and $10 \rightarrow 9$ transitions were identified, each consisting of blended $K = 0$ and 1 components (see Table 1). The $J = 9 \rightarrow 8$ line is shown in Figure 2(e), along with one of its ^{13}C-substituted isotopologues; positions and relative intensities of the $K = 0$ and 1 components are

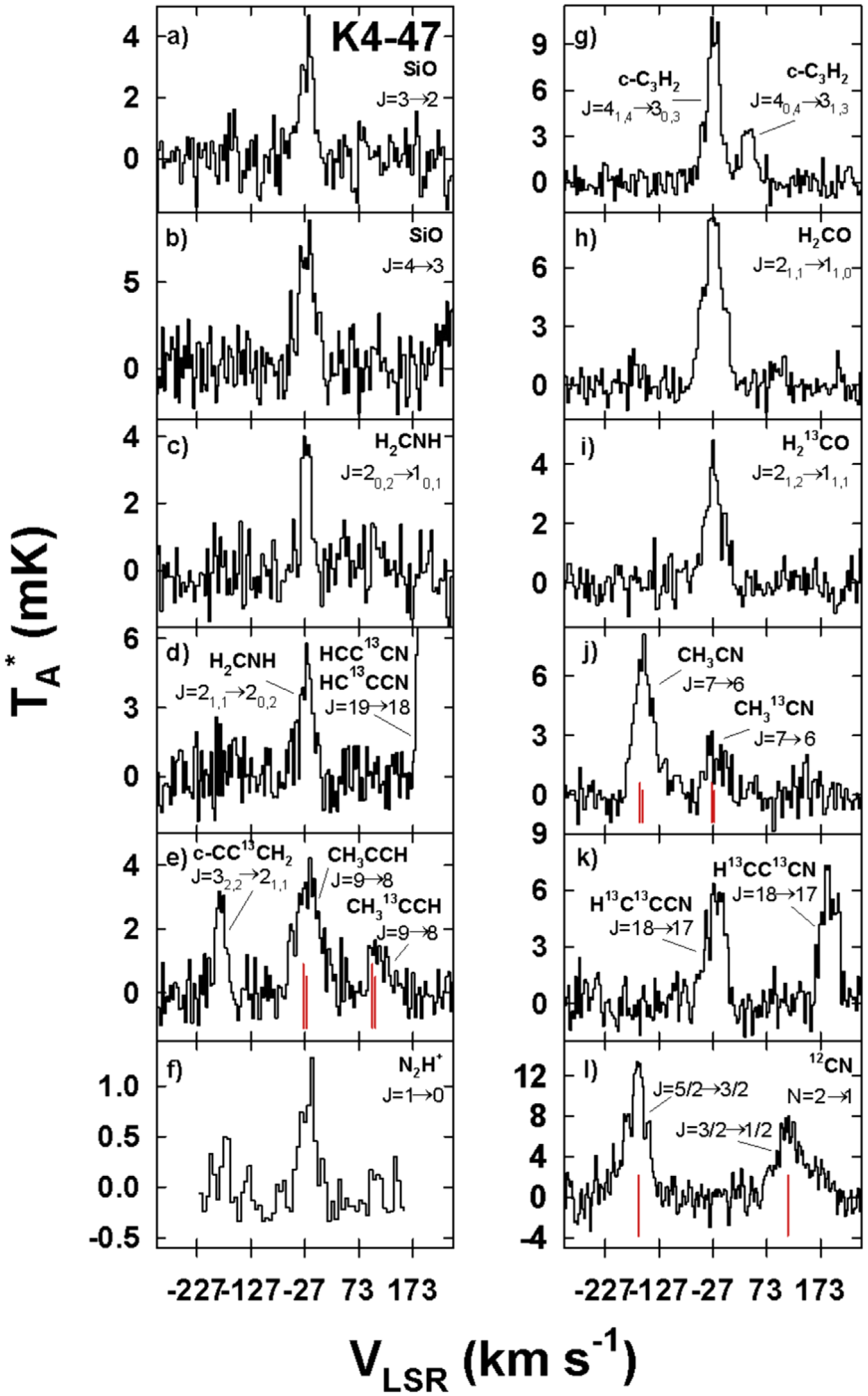

Figure 2. Molecular spectra observed toward K4-47 identified with the IRAM 30 m (2 mm) and ARO telescopes (1 and 3 mm). The spectral resolution is 2 MHz. Left panel, in descending order: (a), (b) $J = 3 \rightarrow 2$ (130.2687 GHz) and $J = 4 \rightarrow 3$ (173.6882 GHz) transitions of SiO; (c), (d) $J_{Ka,Kc} = 2_{0,2} \rightarrow 1_{0,1}$ (127.8568 GHz) and $J_{Ka,Kc} = 2_{1,1} \rightarrow 2_{0,2}$ (172.2671 GHz) transitions of H_2CNH, with a blend of the $J = 19 \rightarrow 18$ lines of $HCC^{13}CN$ and $HC^{13}CCN$ (172.1327 GHz and 172.116 GHz, respectively); (e) $J = 9 \rightarrow 8$ line of CH_3CCH, consisting of blended $K = 0$ and 1 components (average frequency of $K = 0$ and 1 components: 153.8158 GHz; see Table 1), as well as its $CH_3{}^{13}CCH$ isotopologues (average frequency: 153.7519 GHz) and the $J_{Ka,Kc} = 3_{2,2} \rightarrow 2_{1,1}$ transition of c-$CC^{13}CH_2$ (153.8946 GHz); and (f) $J = 1 \rightarrow 0$ line of N_2H^+ (93.1734 GHz). Right panel, in descending order: (g) $J_{Ka,Kc} = 4_{1,4} \rightarrow 3_{0,3}$ (150.8519 GHz) and $J_{Ka,Kc} = 4_{0,4} \rightarrow 3_{1,3}$ (150.8207 GHz) transitions of c-C_3H_2, (h) $J_{Ka,Kc} = 2_{1,1} \rightarrow 1_{1,0}$ line of H_2CO (150.4983 GHz) and (i) $J_{Ka,Kc} = 2_{1,2} \rightarrow 1_{1,1}$ transition of $H_2{}^{13}CO$ (137.450 GHz); (j) $J = 7 \rightarrow 6$ lines of CH_3CN and $CH_3{}^{13}CN$ ($K = 0$ and 1, blended; average frequencies: 128.7782 GHz and 128.7144 GHz, respectively); (k) $J = 18 \rightarrow 17$ transitions of $H^{13}C^{13}CCN$ and $H^{13}CC^{13}CN$ (158.1058 GHz and 157.9845 GHz, respectively), and (l) fine/hyperfine components of the $N = 2 \rightarrow 1$ transition of CN, centered at 226.7684 GHz; fine structure splitting is shown under the spectrum (see Table 1). H_2CNH, CH_3CCH, CH_3CN, and all ^{13}C-substituted species are new detections for PNe.

indicated by red lines under each feature. Confirming $J = 7 \rightarrow 6$ lines of both CH_3CN and $CH_3{}^{13}CN$ are displayed in Figure 2(j), with the $K = 0$ and 1 components denoted with red lines. The figure also shows the two detected transitions of SiO ($J = 3 \rightarrow 2$ and $4 \rightarrow 3$) in Figures 2(a) and (b), as well as additional lines of H_2CO and $H_2{}^{13}CO$ (Figures 2(h) and (i)), and the $J = 1 \rightarrow 0$ transition of N_2H^+(Figure 2(f)). Spectra of various transitions of c-C_3H_2 and c-$CC^{13}CH_2$ are additionally displayed in Figures 2(e) and (g), as well as lines of the singly and doubly substituted ^{13}C isotopologues of HC_3N: see Figures 2(d) and (k).

Table 1
Line Parameters for Main Species Observed in K4-47[a]

Molecule	Telescope	Transition	Frequency (MHz)	T_A^* (mK)	V_{LSR} (km s^{-1})	$\Delta V_{1/2}$ (km s^{-1})	N_{tot} 10^{13} cm^{-2}
CN	12 m	N , $J = 1,3/2 \rightarrow 0,1/2$	113490.9	6.4 ± 1.5	−27.5 ± 2.6	39.0 ± 5.2	24.0 ± 10.0
	SMT	N , $J = 2,3/2 \rightarrow 1,1/2$[b]	226658.7	7.5 ± 2.0	−26.8 ± 3.9	70.0 ± 5.9	
	SMT	N , $J = 2,5/2 \rightarrow 1,3/2$[c]	226875.0	13.0 ± 2.0	−28.0 ± 2.0	42.0 ± 3.9	
SiO	IRAM	$J = 3 \rightarrow 2$	130268.7	4.3 ± 1.5	−25.7 ± 2.0	34.0 ± 3.0	0.4 ± 0.2
	IRAM	$J = 4 \rightarrow 3$	173688.2	7.4 ± 2.2	−26.8 ± 1.7	37.0 ± 4.3	
N_2H^+	12 m	$J = 1 \rightarrow 0$	93173.4	1.2 ± 0.6	−27.0 ± 3.2	25.6 ± 3.2	2.5 ± 1.6
CCH	IRAM	$N,J = 2,5/2 \rightarrow 1,3/2$[d]	174665.4	21.5 ± 2.2	−27.0 ± 1.7	40.0 ± 3.4	22.0 ± 9.0
	IRAM	$N,J = 2,3/2 \rightarrow 1,1/2$[e]	174727.7	13.0 ± 2.2	−27.0 ± 1.7	40.0 ± 4.3	
H_2CO	IRAM	$J_{Ka,Kc} = 2_{0,2} \rightarrow 1_{0,1}$	145602.9	6.8 ± 1.2	−28.5 ± 3.0	37.0 ± 4.0	3.3 ± 0.6
	IRAM	$J_{Ka,Kc} = 2_{1,1} \rightarrow 1_{1,0}$	150498.3	9.0 ± 1.2	−27.5 ± 2.0	39.0 ± 3.0	
	SMT	$J_{Ka,Kc} = 3_{0,3} \rightarrow 2_{0,2}$	218222.2	2.0 ± 0.5	−28.3 ± 2.8	35.0 ± 3.5	
HC_3N	12 m	$J = 9 \rightarrow 8$	81881.5	2.1 ± 0.7	−29.0 ± 3.7	34.0 ± 5.6	6.4 ± 1.1
	IRAM	$J = 14 \rightarrow 13$	127367.7	24.5 ± 1.5	−29.0 ± 2.0	35.0 ± 3.0	
	IRAM	$J = 16 \rightarrow 15$	145561.0	28.5 ± 1.2	−29.0 ± 2.0	39.0 ± 2.0	
	IRAM	$J = 19 \rightarrow 18$	172849.3	35.0 ± 1.5	−27.0 ± 1.7	40.0 ± 4.3	
	SMT	$J = 24 \rightarrow 23$	218324.7	3.7 ± 0.5	−29.0 ± 1.4	40.0 ± 4.2	
c-C_3H_2	12 m	$J_{Ka,Kc} = 2_{1,2} \rightarrow 1_{0,1}$	85338.9	1.3 ± 0.4	−28.0 ± 3.5	30.0 ± 7.0	4.4 ± 1.2
	IRAM	$J_{Ka,Kc} = 3_{1,2} \rightarrow 2_{2,1}$	145089.6	4.2 ± 1.2	−28.0 ± 3.0	33.0 ± 3.0	
	IRAM	$J_{Ka,Kc} = 4_{0,4} \rightarrow 3_{1,3}$	150820.7	4.2 ± 1.2	−27.0 ± 2.0	32.0 ± 4.0	
	IRAM	$J_{Ka,Kc} = 4_{1,4} \rightarrow 3_{0,3}$	150851.9	10.4 ± 1.2	−28.5 ± 2.0	32.0 ± 4.0	
	IRAM	$J_{Ka,Kc} = 5_{1,4} \rightarrow 5_{0,5}$	151343.9	2.5 ± 1.2	−28.0 ± 3.0	30.0 ± 6.0	
	IRAM	$J_{Ka,Kc} = 3_{2,2} \rightarrow 2_{1,1}$	155518.3	3.1 ± 1.2	−28.0 ± 2.0	32.0 ± 4.0	
	SMT	$J_{Ka,Kc} = 3_{3,0} \rightarrow 2_{2,1}$	216278.8	1.3 ± 0.7	−28.7 ± 2.8	32.0 ± 4.2	
H_2CNH	IRAM	$J_{Ka,Kc} = 2_{0,2} \rightarrow 1_{0,1}$	127856.8	4.5 ± 1.5	−27.0 ± 2.0	20.0 ± 3.0	3.0 ± 1.5
	IRAM	$J_{Ka,Kc} = 2_{1,1} \rightarrow 1_{1,0}$	133272.1	2.3 ± 1.2	−27.3 ± 2.0	20.0 ± 4.0	
	IRAM	$J_{Ka,Kc} = 2_{1,1} \rightarrow 2_{0,2}$	172267.1	5.7 ± 2.2	−26.5 ± 2.6	25.0 ± 1.7	
CH_3CN	IRAM	$J = 7 \rightarrow 6$[f]	128778.1	7.3 ± 1.5	−27.0 ± 2.0	42.0 ± 4.0	1.3 ± 0.7
	IRAM	$J = 8 \rightarrow 7$[f]	147173.2	7.4 ± 1.2	−25.0 ± 3.0	43.0 ± 4.0	
CH_3CCH	IRAM	$J = 8 \rightarrow 7$[f]	136726.7	3.8 ± 1.5	−26.0 ± 2.0	43.0 ± 4.0	16.0 ± 6.0
	IRAM	$J = 9 \rightarrow 8$[f]	153815.8	4.4 ± 1.5	−26.0 ± 2.0	41.0 ± 3.0	
	IRAM	$J = 10 \rightarrow 9$[f]	170904.1	6.7 ± 2.0	−27.0 ± 2.6	42.0 ± 2.6	

Notes.
[a] Measured with 1 MHz resolution.
[b] Blend of the $F = 3/2 \rightarrow 1/2$, $F = 5/2 \rightarrow 3/2$, $F = 3/2 \rightarrow 3/2$, and $F = 1/2 \rightarrow 1/2$ hyperfine components.
[c] Blend of the $F = 3/2 \rightarrow 1/2$, $F = 5/2 \rightarrow 3/2$, and $F = 7/2 \rightarrow 5/2$ hyperfine components.
[d] Blend of the $F = 3 \rightarrow 2$ and $F = 2 \rightarrow 1$ hyperfine components.
[e] Blend of the $F = 2 \rightarrow 1$, $F = 1 \rightarrow 0$, and $F = 1 \rightarrow 1$ hyperfine components.
[f] Blend of the $K = 0$ and 1 components.

Finally, two spin-rotation components of the $N = 2 \rightarrow 1$ transition of CN are presented in Figure 2(l), indicated by red lines under the spectrum. The CN profiles appear broader because of blended nitrogen hyperfine structure.

Of additional interest are the surprising number of ^{13}C-substituted species, including $CH_3{}^{13}CN$, c-$CC^{13}CH_2$, $H_2{}^{13}CO$, and doubly substituted HC_3N. Various molecules and their isotopic variants have been reported in our previous observations of K4-47 (HCN, $H^{13}CN$, $HC^{15}N$, HCO^+, HNC, $HN^{13}C$, CO, $C^{17}O$, CS, ^{13}CS, CN, ^{13}CN, HC_3N, $H^{13}CCCN$, $HC^{13}CCN$, and $HCC^{13}CN$; see Schmidt et al. 2018a). The appearance of the series $H^{13}C^{13}CCN$, $HC^{13}C^{13}CN$, and $H^{13}CC^{13}CN$ marks the first time that all three isotopologues have been identified in one source. This result attests to the high enrichment of ^{13}C found in K4-47.

Tables 1 and 2 list the line parameters (T_A^*, V_{LSR}, and $\Delta V_{1/2}$) and column densities N_{tot} of the newly detected species for the main isotopologues and the ^{13}C-substituted species, respectively. The line parameters were determined from Gaussian fits to the line profiles. Column densities were determined using the non-local thermodynamic equilibrium radiative transfer code, RADEX (van der Tak et al. 2007). Here gas kinetic temperature (T_K), H_2 density ($n(H_2)$), and column density are varied to reproduce the observed line intensities. At least three transitions were detected for most molecules, allowing all three parameters to be fit. However, for species for which only one or two transitions were measured, T_K alone, or T_K and $n(H_2)$, were set to that determined from a molecule with a comparable dipole moment (such as CO for ^{13}CO). The line intensities were corrected for beam dilution by applying the source size defined by H_2 emission (Akras et al. 2017). Observations of the Helix Nebula have demonstrated that H_2 and other molecular emission are spatially coincident (Zeigler et al. 2013). The molecular data files used for the analysis were taken from the Leiden Atomic and Molecular Database (LAMDA; Schöier et al. 2005), or generated from molecular data in the CDMS or JPL catalogs; collision rates are from BASECOL (Dubernet et al. 2013). The best fit was determined

Table 2
Line Parameters for Isotopologues Observed in K4-47[a]

Molecule		Transition	Frequency (MHz)	T_A^* (mK)	V_{LSR} (km s^{-1})	$\Delta V_{1/2}$ (km s^{-1})	N_{tot} 10^{13} cm^{-2}
^{13}CO	SMT	$J = 2 \rightarrow 1$	220398.7	69.3 ± 4.7	−27.5 ± 1.4	20.0 ± 2.1	6200.0 ± 1200.0
H^{13}CO$^+$	12 m	$J = 1 \rightarrow 0$	86754.3	2.4 ± 0.4	−28.0 ± 1.7	18.0 ± 3.5	0.9 ± 0.2
	IRAM	$J = 2 \rightarrow 1$[b]	173506.7	51.8 ± 2.2	−28.0 ± 1.7	22.0 ± 1.7	
C^{13}CH	IRAM	$N = 2 \rightarrow 1$[c]	170518.9	5.0 ± 2.0	−27.0 ± 3.4	120.0 ± 10.2	9.9 ± 3.5
H$_2^{13}$CO	IRAM	$J_{Ka,Kc} = 2_{1,2} \rightarrow 1_{1,1}$	137450.0	4.4 ± 1.2	−27.1 ± 3.0	37.0 ± 4.0	1.4 ± 0.5
	IRAM	$J_{Ka,Kc} = 2_{0,2} \rightarrow 1_{0,1}$	141983.7	2.4 ± 1.2	−27.0 ± 2.0	37.0 ± 5.1	
	IRAM	$J_{Ka,Kc} = 2_{1,1} \rightarrow 1_{1,0}$	146635.7	4.0 ± 1.5	−26.0 ± 3.0	37.0 ± 6.0	
H^{13}CCCN	12 m	$J = 10 \rightarrow 9$	88166.8	1.8 ± 0.4	−28.3 ± 3.5	38.0 ± 3.5	3.1 ± 0.7
	IRAM	$J = 18 \rightarrow 17$	158692.0	14.7 ± 1.5	−27.5 ± 1.7	35.0 ± 2.6	
	IRAM	$J = 20 \rightarrow 19$	176321.3	15.8 ± 2.2	−29.8 ± 1.7	38.0 ± 3.4	
HC^{13}CCN	IRAM	$J = 14 \rightarrow 13$	126827.3	12.0 ± 1.5	−28.0 ± 2.0	37.0 ± 2.0	3.1 ± 0.7
	IRAM	$J = 16 \rightarrow 15$	144943.5	16.0 ± 1.5	−27.7 ± 2.0	37.0 ± 3.0	
	IRAM	$J = 19 \rightarrow 18$	172116.0	16.5 ± 1.5	−28.8 ± 2.6	39.0 ± 5.1	
	SMT	$J = 24 \rightarrow 23$	217398.6	2.5 ± 0.9	−29.2 ± 2.8	37.0 ± 4.2	
HCC^{13}CN	IRAM	$J = 14 \rightarrow 13$	126839.6	12.0 ± 1.5	−29.0 ± 2.0	37.0 ± 2.0	3.1 ± 0.6
	IRAM	$J = 16 \rightarrow 15$	144957.5	16.0 ± 1.5	−29.2 ± 2.0	37.0 ± 3.0	
	IRAM	$J = 19 \rightarrow 18$	172132.7	16.0 ± 1.5	−27.9 ± 2.6	39.0 ± 3.4	
	SMT	$J = 24 \rightarrow 23$	217419.6	2.5 ± 0.9	−27.3 ± 2.8	37.0 ± 4.2	
H^{13}C^{13}CCN	IRAM	$J = 15 \rightarrow 14$	131757.8	5.2 ± 1.0	−28.5 ± 2.0	37.0 ± 3.0	1.2 ± 0.4
	IRAM	$J = 17 \rightarrow 16$	149323.4	5.4 ± 1.5	−29.5 ± 2.0	38.0 ± 4.0	
	IRAM	$J = 18 \rightarrow 17$	158105.8	6.7 ± 1.5	−27.0 ± 2.6	34.0 ± 5.1	
	IRAM	$J = 20 \rightarrow 19$	175670.0	5.7 ± 2.2	−29.7 ± 5.1	35.0 ± 2.6	
H^{13}CC^{13}CN	IRAM	$J = 15 \rightarrow 14$	131656.8	5.5 ± 1.5	−29.0 ± 2.0	35.0 ± 3.0	1.3 ± 0.5
	IRAM	$J = 17 \rightarrow 16$	149208.8	6.3 ± 1.5	−27.0 ± 2.0	39.0 ± 3.0	
	IRAM	$J = 18 \rightarrow 17$	157984.5	6.7 ± 1.5	−27.0 ± 2.6	34.0 ± 5.1	
	IRAM	$J = 20 \rightarrow 19$	175535.2	5.5 ± 2.2	−27.5 ± 2.6	37.0 ± 3.4	
HC^{13}C^{13}CN	IRAM	$J = 14 \rightarrow 13$	126283.2	6.3 ± 1.5	−28.3 ± 2.0	37.0 ± 3.0	1.7 ± 0.6
	IRAM	$J = 15 \rightarrow 14$	135302.5	6.6 ± 1.5	−25.5 ± 2.0	35.0 ± 2.0	
	IRAM	$J = 16 \rightarrow 15$	144321.5	5.8 ± 1.5	−28.0 ± 2.0	37.0 ± 4.0	
	IRAM	$J = 17 \rightarrow 16$	153340.4	5.5 ± 1.5	−26.8 ± 2.0	37.0 ± 4.0	
	IRAM	$J = 19 \rightarrow 18$	171377.5	6.6 ± 2.2	−27.2 ± 1.7	37.0 ± 2.6	
c-^{13}CCCH$_2$	IRAM	$J_{Ka,Kc} = 4_{1,4} \rightarrow 3_{0,3}$	147069.7	2.1 ± 1.2	−26.0 ± 5.0	35.0 ± 5.0	0.7 ± 0.4
c-CC^{13}CH$_2$	IRAM	$J_{Ka,Kc} = 4_{0,4} \rightarrow 3_{1,3}$	148051.8	4.3 ± 1.2	−26.8 ± 3.0	30.0 ± 5.0	1.7 ± 0.6
	IRAM	$J_{Ka,Kc} = 4_{1,4} \rightarrow 3_{0,3}$	148114.2	4.3 ± 1.2	−27.0 ± 4.0	30.0 ± 5.0	
	IRAM	$J_{Ka,Kc} = 3_{2,2} \rightarrow 2_{1,1}$	153894.6	3.3 ± 1.5	−28.0 ± 2.0	30.0 ± 4.0	
CH$_3^{13}$CN	IRAM	$J = 7 \rightarrow 6$[d]	128714.4	2.7 ± 1.5	−25.0 ± 6.0	42.0 ± 6.0	0.5 ± 0.2
	IRAM	$J = 8 \rightarrow 7$[d]	147100.4	3.8 ± 1.2	−28.0 ± 4.0	42.0 ± 6.0	
^{13}CH$_3$CN	IRAM	$J = 8 \rightarrow 7$[d]	142924.2	2.4 ± 1.2	−27.0 ± 3.1	43.0 ± 5.1	0.4 ± 0.2
	IRAM	$J = 9 \rightarrow 8$[d]	160787.4	3.4 ± 1.5	−29.0 ± 1.7	42.0 ± 4.3	
CH$_3^{13}$CCH	IRAM	$J = 8 \rightarrow 7$[d]	136670.0	2.1 ± 1.5	−25.0 ± 3.0	38.0 ± 5.0	7.4 ± 3.0
	IRAM	$J = 9 \rightarrow 8$[d]	153751.9	2.1 ± 1.5	−25.0 ± 4.0	38.0 ± 5.0	
	IRAM	$J = 10 \rightarrow 9$[d]	170833.3	2.7 ± 2.0	−27.0 ± 5.1	38.0 ± 5.1	
^{13}CH$_3$CCH	IRAM	$J = 9 \rightarrow 8$[d]	149628.9	2.0 ± 1.2	−25.5 ± 2.0	42.0 ± 4.9	7.0 ± 4.6

Notes.
[a] Measured with 1 MHz resolution.
[b] Weak (∼22 mK) plateau feature also present; see Edwards et al. (2014).
[c] Blend of the $J = 5/2 \rightarrow 3/2$ and $J = 3/2 \rightarrow 1/2$ spin rotation components.
[d] Blend of the $K = 0$ and 1 components.

by a χ^2 analysis. Typical gas densities and kinetic temperatures of $\sim 1 \times 10^6$ cm^{-2} and ∼65 K were consistently found.

Table 3 summarizes all molecular species now identified in K4-47, their observed isotopic variants, and fractional abundances for the main species. The list currently totals 16 different chemical compounds, including H_2, and 22 isotopically substituted species with ^{13}C, ^{17}O, or ^{15}N. Fractional abundances with respect to H_2 were determined by using the molecular hydrogen column density of 2.9×10^{20} cm^{-2} derived by Edwards et al. (2014). The $^{12}C/^{13}C$ ratios established from the respective chemical compounds are also listed. The ratios are remarkably uniform, with values in the range $^{12}C/^{13}C \sim 1.3$–6.3.

4. Discussion

4.1. K4-47: The Most Chemically Complex PN to Date

These observations demonstrate that K4-47 is the most chemically rich PN currently known, with the identification of 16 different chemical species, including several with five to seven atoms. Many of these molecules such as N_2H^+, H_2CO, HC_3N, and SiO have only been seen in a few other PNe. For

Table 3
Molecules Identified in K4-47

Molecule	Isotopic Variations	Abundances[a]	$^{12}C/^{13}C$ Ratios
H_2			
CO	^{13}CO, $C^{17}O$	7.2×10^{-4}	3.4
CS	^{13}CS	6.2×10^{-8}	4.6
CN	^{13}CN	8.3×10^{-7}	1.7
SiO		1.4×10^{-8}	
HCN	$H^{13}CN$, $HC^{15}N$	5.2×10^{-7}	1.8
HNC	$HN^{13}C$	1.1×10^{-7}	1.3
HCO^+	$H^{13}CO^+$	4.8×10^{-8}	1.5
CCH	$C^{13}CH$	7.6×10^{-7}	2.2
N_2H^+		8.6×10^{-8}	
H_2CO	$H_2{}^{13}CO$	1.1×10^{-7}	2.4
HC_3N	$H^{13}CCCN$, $HCC^{13}CN$, $HC^{13}CCN$, $HC^{13}C^{13}CN$, $H^{13}CC^{13}CN$, $H^{13}C^{13}CCN$	2.2×10^{-7}	2.1[b]
$c\text{-}C_3H_2$	$c\text{-}^{13}CCCH_2$, $c\text{-}CC^{13}CH_2$	1.5×10^{-7}	2.6–6.3
H_2CNH		1.0×10^{-7}	
CH_3CN	$CH_3{}^{13}CN$, $^{13}CH_3CN$	4.5×10^{-8}	2.6–3.3
CH_3CCH	$CH_3{}^{13}CCH$, $^{13}CH_3CCH$	5.5×10^{-7}	2.2–2.3

Notes.
[a] Abundances are given for the main isotopologue only.
[b] Singly substituted ^{13}C isotopologues only.

example, H_2CO has been definitively identified toward NGC 6537 and the Helix Nebula (Edwards & Ziurys 2013; Zack & Ziurys 2013), while HC_3N has been previously observed exclusively in NGC 7027 (Zhang et al. 2008). The O-rich nebula M2-48 has been the only PN until now where SiO has been detected; NGC 6537, NGC 7027, and M2-48 are the three other conclusive sources of N_2H^+ (Zhang et al. 2008; Edwards & Ziurys 2013, 2014). CH_3CN, H_2CNH, and CH_3CCH are completely new identifications for PNe, as mentioned.

The most prevalent molecules in K4-47, after H_2 and CO, are the radicals CCH and CN, which have abundances of $f \sim 8 \times 10^{-7}$, where f represents the molecular fractional abundance relative to molecular hydrogen. Surprisingly, the next most abundant molecule is CH_3CCH, which has $f \sim 6 \times 10^{-7}$, followed by HCN ($f \sim 5 \times 10^{-7}$), and then HC_3N ($f \sim 2 \times 10^{-7}$). H_2CO, $c\text{-}C_3H_2$, H_2CNH, and HNC all have comparable abundances of $\sim 10^{-7}$. Less prevalent are the molecular ions $HCO^+$and N_2H^+, which have $f \sim 5\text{–}9 \times 10^{-8}$, as do CH_3CN and CS. The least abundant species is SiO ($f \sim 10^{-8}$), as expected in this C-rich source. Carbon-bearing compounds clearly dominate the chemistry of K4-47, with simple chains and rings. C–N bonds are also common, suggesting an enhancement of nitrogen, as does the presence of N_2H^+. However, $[CH_3CCH]/[CH_3CN] \sim 12$, suggesting carbon controls the chemistry, not nitrogen.

The estimated molecular abundances are typically larger in K4-47 than in other PNe, although such results are dependent on the estimated source size. A $30'' \times 20''$ source was assumed for M2-48, as deduced from CO mapping (Edwards & Ziurys 2014); for NGC 6537, $30''$ was employed, based on its optical image (Edwards & Ziurys 2013). Large-scale HCO^+ maps clearly show that molecular emission is extended in the Helix Nebula (Zeigler et al. 2013). Formaldehyde has been definitively identified toward NGC 6537 and across the Helix Nebula with abundances of $\sim 2.2 \times 10^{-8}$ and $0.25\text{-}2.1 \times 10^{-7}$, respectively (Edwards & Ziurys 2013; Zack & Ziurys 2013)—on average lower than in K4-47. Interestingly, Edwards & Ziurys (2013) attributed the presence of H_2CO in both objects to their slight oxygen-rich nature (C ~ O). In contrast, K4-47 is very carbon-rich, similar to NGC 7027, but H_2CO is apparently absent from the latter source. Furthermore, HC_3N has been detected in only one other PN, NGC 7027 (Zhang et al. 2008), with an abundance of 8.5×10^{-9}—about a factor of 30 lower than that of K4-47. The N_2H^+ abundances for NGC 6537 and NGC 7027 are notably less than that of K4-47 by factors of ~10–20 (7.8×10^{-9} and 3.8×10^{-9}, respectively: Zhang et al. 2008; Edwards & Ziurys 2013). This ion, however, is slightly more prevalent in M2-48 (9.8×10^{-8}; Edwards & Ziurys 2014). SiO is also a factor of 2 more abundant in M2-48 than K4-47, with $f \sim 2.9 \times 10^{-8}$. K4-47 additionally has some of the highest abundances among PNe for HCN, CCH, HNC, and HCO^+ (Schmidt & Ziurys 2016, Schmidt & Ziurys 2017a, 2017b).

K4-47 also exhibits ~10 unidentified lines, based on very limited frequency coverage, although a few may be attributable to H_2CN. U-lines are not commonly observed in PNe. Those found in K4-47 have thus far defied identification.

4.2. The Carbon-chemistry Sequence: From IRC+10216 to K4-47?

All the chemical compounds detected in K4-47 have been observed in the envelope of IRC+10216, the canonical carbon-rich AGB star, with the exception of N_2H^+. Some of the rarer ^{13}C isotopologues such as $H^{13}CO^+$and $H_2{}^{13}CO$ are absent from IRC+10216, as well. In general, the abundances of most molecules are higher in IRC+10216 than K4-47. For example, SiO, HCN, CCH, and HC_3N are factors of 12, 25, 4, and 4 more prevalent in the AGB envelope, respectively (e.g., Woods et al. 2003; Schöier et al. 2006; Zhang et al. 2017). There are exceptions however, involving ions or more complex organic species. HCO^+, H_2CO, and CH_3CCH are all more abundant in K4-47 by about an order of magnitude, and H_2CNH by at least a factor of 3 (e.g., Ford et al. 2004; Agúndez et al. 2008; Tenenbaum et al. 2010; Pulliam et al. 2011).

Another relevant source is the C-rich PPN CRL 618. This object contains an almost identical set of molecules as K4-47, including the ions $HCO^+$and N_2H^+, as well as some of the doubly substituted HC_3N species absent from IRC+10216, $H^{13}CC^{13}CN$, and $HC^{13}C^{13}CN$ (e.g., Pardo & Cernicharo 2007; Lee et al. 2013a). H_2CNH and other ^{13}C-substituted species such as $H^{13}C^{13}CCN$ and $CH_3{}^{13}CCH$, however, have not been observed in CRL618. The abundances for CRL 618 are generally comparable to those measured in K4-47 for HCN, HNC, HCO^+, and HC_3N (Sánchez-Contreras et al. 2004; Pardo & Cernicharo 2007). On the other hand, several species are particularly prevalent in K4-47, including CH_3CCH, CH_3CN, and CCH, whose abundances are higher than those in CRL 618 by factors of ~13, ~6, and ~7, respectively (Pardo & Cernicharo 2007).

The similarity of molecular species among IRC+10216, CRL 618, and K4-47 suggests an evolutionary sequence. The neutral carbon chemistry that dominates the AGB becomes altered as UV radiation from the developing white dwarf in the PPN and then PN phases enhances the production of molecular ions. In addition, the photodestruction of abundant molecules such as HCN and HC_3N produces C-bearing fragments that may react to create species such as CH_3CCH. Indeed, an evolutionary connection between IRC+10216 and CRL 618 is already established (e.g., Herpin et al. 2002), with abundances of various molecular species changing with temperature, density, and the ambient UV field. Furthermore, K4-47 and

CRL 618 have similar collimated, bipolar outflows with scale sizes ∼0.04–0.3 pc (Corradi et al. 2000; Lee et al. 2013b). Moreover, the expansion velocities of these two outflows are comparable at $\sim$150 km s^{-1} for K4-47 and $\sim$340 km s^{-1} for CRL 618 (Corradi et al. 2000; Sánchez-Contreras et al. 2017).

4.3. The Effects of Nucleosynthesis

The evolutionary sequence from the AGB to the PN phase is also reflected in the respective C, N, and O isotope ratios. With $^{12}C/^{13}C = 2.2 \pm 0.8$, $^{14}N/^{15}N = 13.6 \pm 6.5$, and $^{16}O/^{17}O = 21.4 \pm 10.3$ (Schmidt et al. 2018a), the isotope enhancement of ^{13}C, ^{15}N, and ^{17}O in K4-47 is clearly colossal. However, CRL 618 exhibits similar, although not as extreme, enrichments with $^{12}C/^{13}C \sim 9$ and $^{14}N/^{15}N \sim 150$ in its dense core (Lee et al. 2013a). A decidedly subsolar $^{16}O/^{17}O$ ratio of ∼242 was also measured in this source by Kahane et al. (1992). The $^{12}C/^{13}C$, $^{14}N/^{15}N$, and $^{16}O/^{17}O$ ratios measured in IRC+10216, on the other hand, appear to reflect expected AGB nucleosynthesis. The $^{12}C/^{13}C$ ratio of ∼25–50 is much higher than the CNO equilibrium value of ∼3–4, indicative of the triple alpha process converting He to ^{12}C, followed by dredge up (Milam et al. 2009). The $^{16}O/^{17}O$ ratio of ∼967 is somewhat enhanced in ^{17}O (He et al. 2008), reflecting CNO enrichment of this isotope (Straniero et al. 2017), while the large $^{14}N/^{15}N \sim$ 1800–3600 results from dilution by ^{14}N in the CNO cycle; note that the CNO equilibrium value is $^{14}N/^{15}N \sim$ 30,000.

The enrichment of ^{13}C, ^{15}N, and ^{17}O in both K4-47 and CRL 618 suggests that both objects may have evolved from J-type stars that underwent an explosive process at the end of the AGB. J-type stars are C-rich and exhibit an enhanced $^{12}C/^{13}C$ ratio close to the CNO-cycle equilibrium value (e.g., Abia et al. 2017). Enrichment in carbon occurs through the triple alpha process, which raises the $^{12}C/^{13}C$ ratio. J-type stars are thus an enigma. The enhancement of ^{15}N and ^{17}O in K4-47 and CRL 618 may have occurred via a He-shell flash. In this scenario, the flash injects ^{12}C from the He-burning shell into the H-burning shell, leading to hot CNO reactions that produce ^{13}C, ^{15}N, and ^{17}O. This explosive process ejects these products from the H-shell before competing reactions destroy them, leading to the extreme bipolar morphology of these objects. Lee et al. (2013a) proposed a similar scheme for CRL 618, which involves a hot CNO cycle in a nova-like explosion, leading to bullet-like ejections observed in the PPN.

Huang et al. (2016) stated that a nova-like origin for the ratios in CRL 618 would necessitate a binary system with a secondary white dwarf, though the helium shell flash phenomenon would not. While the central star of CRL 618 cannot be directly observed at optical wavelengths, Balick et al. (2014) found evidence of an active symbiotic system with a donor AGB and WC8 stars. There is currently no evidence for a symbiotic system for K4-47. On the other hand, similar isotope ratios and molecular content are found for CK Vul, also postulated to be a stellar merger (Kamiński et al. 2017).

This work is supported by NSF grant AST-1515568. We thank the staff of ARO and IRAM for their support.

References

Abia, C., Hedrosa, R. P., Domínguez, I., & Straniero, O. 2017, A&A, 599, A39
Agúndez, M., Fonfría, J. P., Cernicharo, J., Pardo, J. R., & Guélin, M. 2008, A&A, 479, 493
Akras, S., Gonçalves, D. R., & Ramos-Larios, G. 2017, MNRAS, 465, 1289
Balick, B., Riera, A., Raga, A., Kwitter, K. B., & Velázquez, P. F. 2014, ApJ, 795, 83
Cami, J., Bernard-Salas, J., Peeters, E., & Malek, S. E. 2010, Sci, 329, 1180
Corradi, R., Gonçalves, D. R., Villaver, E., et al. 2000, ApJ, 535, 823
Dubernet, M. L., Alexander, M. H., Ba, Y. A., et al. 2013, A&A, 553, A50
Edwards, J. L., Cox, E. G., & Ziurys, L. M. 2014, ApJ, 791, 79
Edwards, J. L., & Ziurys, L. M. 2013, ApJL, 770, L5
Edwards, J. L., & Ziurys, L. M. 2014, ApJL, 794, L27
Endres, C. P., Schlemmer, S., Schilke, P., Stutzki, J., & Müller, H. S. P. 2016, JMoSp, 327, 95
Ford, K. E. S., Neufeld, D. A., Schilke, P., & Melnick, G. J. 2004, ApJ, 614, 990
García-Hernández, D. A., Villaver, E., García-Lario, P., et al. 2012, ApJ, 760, 107
He, J. H., Dinh-V-Trung, Kwok, S., et al. 2008, ApJSS, 177, 275
Herpin, F., Goicoechea, J. R., Pardo, J. R., & Cernicharo, J. 2002, ApJ, 577, 961
Huang, P.-S., Lee, C.-F., Moraghan, A., & Smith, M. 2016, ApJ, 820, 134
Huggins, P. J., Bachiller, R., Planesas, P., Forveille, T., & Cox, P. 2005, ApJSS, 160, 272
Kahane, C., Cernicharo, J., Gómez-González, J., & Guélin, M. 1992, A&A, 256, 235
Kamiński, T., Menten, K. M., Tylenda, R., et al. 2017, A&A, 607, A78
Lee, C., Yang, C., Sahai, R., & Sánchez Contreras, C. 2013a, ApJ, 770, 153
Lee, C.-F., Sahai, R., Sánchez Contreras, C., Huang, P.-S., & Jian Hao Tay, J. 2013b, ApJ, 777, 37
Lumsden, S. L., Puxley, P. J., & Hoare, M. G. 2001, MNRAS, 328, 419
Meaburn, J., Lopez, J. A., & Richer, M. G. 2008, MNRAS, 384, 497
Milam, S. N., Woolf, N. J., & Ziurys, L. M. 2009, ApJ, 690, 837
Müller, H. S. P., Schlöder, F., Stutzki, J., & Winnewisser, G. 2005, J. Mol. Struct., 742, 215
Müller, H. S. P., Thorwirth, S., Roth, D. A., & Winnewisser, G. 2001, A&A, 370, L49
Pardo, J. R., & Cernicharo, J. 2007, ApJ, 654, 978
Pickett, H. M., Poynter, R. L., Cohen, E. A., et al. 1998, JQSRT, 60, 883
Pulliam, R. L., Edwards, J. L., & Ziurys, L. M. 2011, ApJ, 743, 36
Redman, M. P., Viti, S., Cau, P., & Williams, D. A. 2003, MNRAS, 345, 1291
Sánchez-Contreras, C., Báez-Rubio, A., Alcolea, J., Bujarrabal, V., & Martín-Pintado, J. 2017, A&A, 603, A67
Sánchez-Contreras, C., Bujarrabal, V., Castro-Carrizo, A., Alcolea, J. K., & Sargent, A. 2004, ApJ, 617, 1142
Schmidt, D. R., Woolf, N. J., Zega, T. J., & Ziurys, L. M. 2018a, Natur, 564, 378
Schmidt, D. R., Zack, L. N., & Ziurys, L. M. 2018b, ApJL, 864, L31
Schmidt, D. R., & Ziurys, L. M. 2016, ApJ, 817, 175
Schmidt, D. R., & Ziurys, L. M. 2017a, ApJ, 835, 79
Schmidt, D. R., & Ziurys, L. M. 2017b, ApJ, 850, 123
Schöier, F. L., Fong, D., Olofsson, H., Zhang, Q., & Patel, N. 2006, ApJ, 649, 965
Schöier, F. L., van der Tak, F. F. S., van Dishoeck, E. F., & Black, J. H. 2005, A&A, 432, 369
Straniero, O., Bruno, C. G., Aliotta, M., et al. 2017, A&A, 598, A128
Tenenbaum, E. D., Dodd, J. L., Milam, S. N., Woolf, N. J., & Ziurys, L. M. 2010, ApJL, 720, L102
van der Tak, F. F. S., Black, J. H., Schöier, F. L., Jansen, D. J., & van Dishoeck, E. F. 2007, A&A, 468, 627
Woods, P. M., Schöier, F. L., Nyman, L.-Å., & Olofsson, H. 2003, A&A, 402, 617
Zack, L. N., & Ziurys, L. M. 2013, ApJ, 765, 112
Zeigler, N. R., Zack, L. N., Woolf, N. J., & Ziurys, L. M. 2013, ApJ, 778, 16
Zhang, X.-Y., Zhu, Q.-F., Li, J., et al. 2017, A&A, 606, A74
Zhang, Y., Kwok, S., & Dinh-V-Trung 2008, ApJ, 678, 328